Effect of Confinement on Capillary Phase Transition in Granular Aggregates

Citation: Siavash Monfared, Tingtao Zhou, José E. Andrade, Katerina Ioannidou, Farhang Radjaï, Franz-Josef Ulm, and Roland J.-M. Pellenq, Effect of Confinement on Capillary Phase Transition in Granular Aggregates, Phys. Rev. Lett. 125, 255501

As Published: 10.1103/PHYSREVLETT.125.255501

Publisher: American Physical Society (APS)

Persistent URL: https://hdl.handle.net/1721.1/133080

Version: Final published version: final published article, as it appeared in a journal, conference proceedings, or other formally published context

Effect of Confinement on Capillary Phase Transition in Granular Aggregates

Siavash Monfared,[1,*] Tingtao Zhou,[1,†] José E. Andrade,[1,‡] Katerina Ioannidou,[2,3,§] Farhang Radjaï,[2,‖] Franz-Josef Ulm,[4,¶] and Roland J.-M. Pellenq[5,3,**]

[1]*Division of Engineering and Applied Science, California Institute of Technology, Pasadena, California 91125, USA*
[2]*CNRS, University of Montpellier, LMGC, 163 rue Auguste Broussonnet F-34090 Montpellier, France*
[3]*MultiScale Material Science for Energy and Environment UMI 3466 CNRS-MIT-Aix-Marseille Université Joint Laboratory, Cambridge, Massachusetts 02139, USA*
[4]*Department of Civil and Environmental Engineering, Massachusetts Institute of Technology, Cambridge, Massachusetts 02139, USA*
[5]*Department of Physics, Georgetown University, Washington, D.C. 20057, USA*

(Received 10 August 2020; accepted 16 November 2020; published 15 December 2020)

Using a 3D mean-field lattice-gas model, we analyze the effect of confinement on the nature of capillary phase transition in granular aggregates with varying disorder and their inverse porous structures obtained by interchanging particles and pores. Surprisingly, the confinement effects are found to be much less pronounced in granular aggregates as opposed to porous structures. We show that this discrepancy can be understood in terms of the surface-surface correlation length with a connected path through the fluid domain, suggesting that this length captures the true degree of confinement. We also find that the liquid-gas phase transition in these porous materials is of second order nature near capillary critical temperature, which is shown to represent a true critical temperature, i.e., independent of the degree of disorder and the nature of the solid matrix, discrete or continuous. The critical exponents estimated here from finite-size scaling analysis suggest that this transition belongs to the 3D random field Ising model universality class as hypothesized by F. Brochard and P.G. de Gennes, with the underlying random fields induced by local disorder in fluid-solid interactions.

DOI: 10.1103/PhysRevLett.125.255501

The fluid behavior confined in a solid matrix is of interest to a range of scientific and engineering fields, including wet granular physics and poromechanics [1–3], plant biology [4,5], carbon capture technologies [6], catalysis [7,8], and optics [9]. The behavior of a confined fluid contrasts significantly with that of a bulk fluid. This is a consequence of pore morphology, topology, and the relative strength of fluid-solid to fluid-fluid interactions that alter the energy landscape of a fluid [10–17]. In particular, the degree to which a fluid experiences confinement results in a shifted liquid-gas phase transition [12,18,19]. This effect is best captured through the concept of "capillary criticality" that hinges on the existence of a temperature T_{cc} below the bulk critical temperature beyond which liquid-gas phase transitions become reversible.

For disordered porous materials, the nature of liquid-gas phase transitions and the question of whether capillary criticality is associated with a true critical point, i.e., termination of the liquidus line, are still unclear [20,21]. Additionally, a central issue is how the effective random fields induced by structural and/or chemical disorder affect the degree of confinement and critical exponents and thus the universality class classification. Bulk liquid-gas phase transitions are generally in the same universality class as the Ising ferromagnet [22,23]. It was conjectured by F. Brochard and P.G. de Gennes that the universality class of liquid-gas phase transitions in disordered porous materials should be that of the random-field Ising model (RFIM) [24,25]. This argument is built on the stochastic nature of effective wall separation in disordered porous media that manifests itself as a quenched random variable in space.

Inspired by analogies between jammed granular packings and disordered porous solids highlighted recently via studies on the mechanics of dry systems [26,27], we explore in this Letter the capillary phase transition in granular aggregates (discrete) and their inverse porous structures as obtained by interchanging pores and particles (continuous). Based on extensive lattice-gas simulations, we examine (1) whether T_{cc} represents a true critical temperature, (2) the nature of phase transition as $T \to T_{cc}$, and (3) Brochard and de Gennes' hypothesis [24,25] that the critical behavior of fluids in random porous media can be mapped into the RFIM [28] universality class. This has been only confirmed in colloid-polymer mixtures confined in random porous media and via Monte Carlo simulations [29–31]. As we shall see, the confinement effects differ in the two types of structure, but in both cases Brochard and de Gennes' hypothesis holds and T_{cc} appears to be a true critical temperature.

Let us consider a set of granular media (GM) composed of rigid, nonoverlapping monodisperse spherical particles, each confined to a cubic box of size $L_x = L_y = L_z = 80$ nm with

a reservoir of length $L_{\mathrm{res}} = 5$ nm added in all directions. The first three structures A, B, C have $N_p = 512$ particles with radius $R = 4.7$ nm and a packing fraction of $f_s = 0.43$ but exhibit contrasting pore sizes (r_p), distributions (PSD), and increasingly more spatial disorder. Structure D, which has $N_p = 955$ particles and radius $R = 4$ nm, exhibits a degree of spatial disorder similar to that of structure C but a packing fraction of $f_s = 0.5$ (see Supplemental Material for porous structure generation and PSD characterization [32]). The corresponding inverse or "negative" structures are porous solids (PS) obtained by switching pores and particles. We also consider a set of cylindrical pores (CP) of length $L_x = 160$ nm $\ll L_y = L_z$ with pore radius $r_p \in \{2, 4, 8\}$ nm and with reservoirs of length $L_{\mathrm{res}} = 4$ nm added to both ends.

We use a parallelized implementation of coarse-grained lattice gas density functional theory (CGLT) [44,45] with periodic boundary conditions in all directions on a simple cubic lattice with coordination number $c = 6$. In this mean-field approach, the fluid is modeled in the grand canonical ensemble via minimizing the grand potential Ω with the normalized density field $\rho(\vec{x})$ serving as the only order parameter in the model:

$$\Omega = -w_{ff}\sum_{\langle i,j\rangle}\rho_i\rho_j - w_{sf}\sum_{i,j}\rho_i\eta_j - \mu\sum_i\rho_i + k_BT\sum_i[\rho_i\ln(\rho_i) + (1-\rho_i)\ln(1-\rho_i)], \quad (1)$$

where $\eta_i = 0(=1)$ indicates occupancy of site i with solid (fluid). w_{ff} and w_{sf} represent fluid-fluid and solid-fluid energy interaction parameters where $y = w_{sf}/w_{ff}$ is set to $y = 2.5$, corresponding to a strong solid-fluid surface affinity akin to methane in porous carbon or water in cement [46].

Based on our lattice choice, the normalized bulk critical temperature $\bar{T}_c^{3\mathrm{D}} = k_BT_c^{3\mathrm{D}}/w_{ff} = c/4 = 1.5$, and the normalized chemical potential corresponding to bulk liquid-gas phase transition $\bar{\mu}_{\mathrm{sat}}^{3\mathrm{D}} = \mu_{\mathrm{sat}}^{3\mathrm{D}}/w_{ff} = -c/2 = -3$ is set. In the continuum limit and with correct parameterization, CGLT [Eq. (1)] approaches the Cahn-Hilliard model [47,48], paving the way to capture the liquid-gas interface diffusively [49,50]. This provides access to capillary stresses as a tensorial field, $\boldsymbol{\sigma}(\vec{x})$, via a Kortweg stress definition [51,52] and subsequently a capillary pressure scalar field, $p(\vec{x}) = (1/3)tr\boldsymbol{\sigma}(\vec{x})$ (see Supplemental Material [32]):

$$\boldsymbol{\sigma} = \left[p_0(\rho) - \frac{\kappa}{2}(\vec{\nabla}\rho)^2\right]\boldsymbol{I} + \kappa\vec{\nabla}\rho\otimes\vec{\nabla}\rho + \boldsymbol{\sigma_0}, \quad (2)$$

where $p_0(\rho) = \mu\rho + (cw_{ff}/2)\rho^2 - k_BT[\rho\ln(\rho) + (1-\rho)\times\ln(1-\rho)]$ is the asymptotic bulk value of the hydrostatic pressure, $\boldsymbol{I}$ is the identity tensor, $\boldsymbol{\sigma_0}$ represents an arbitrary constant tensor, $\kappa = a_0^2w_{ff}$, and a_0 denotes lattice spacing.

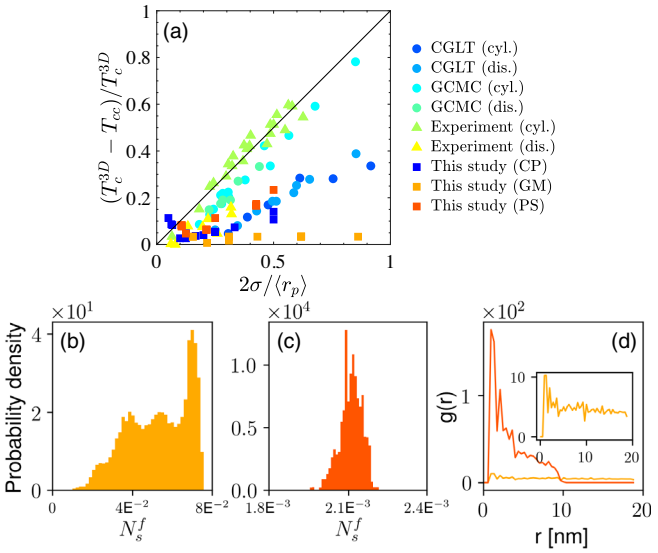

FIG. 1. The degree of confinement represented by (a) shift in capillary critical temperature T_{cc} as a function of the ratio $2\sigma/\langle r_p\rangle$. Previous simulations (circle) and experimental (triangle) data from the literature [58] along with our results (square) for all the considered cylindrical pores (CP), porous solids (PS), and granular media (GM) and for various space discretizations a_0, where $a_0 \sim \sigma$. (b), (c) $N_s^f(r = 20\ \mathrm{nm})$ of GM and PS, respectively, for structure C. (d) Partial radial distribution function for a fluid site at the pore-solid interface with a connected path to a solid site at the pore-solid interface.

For proper energy scaling in this mean-field approach, a_0 is determined from liquid-gas surface tension.

Figure 1(a) displays the calculated shift in critical temperature for GM, PS, and CP as a function of the ratio $2\sigma/\langle r_p\rangle$, with σ denoting the characteristic diameter of a fluid molecule set equal to lattice spacing a_0. It also shows the data from experiments [11,53,54] and previous simulations based on CGLT and grand canonical Monte Carlo (GCMC) for cylindrical pores [55–57], e.g., MCM-41, carbon nanotube, and disordered porous solids, i.e., Vycor, and for a variety of substances such as xenon, argon, and water. The one-to-one scaling between the shift in capillary critical temperature and inverse mean pore size suggests similar behaviors independently of fluid and solid properties and pore connectivity. In this vein, we determine T_{cc} with a resolution of $\approx$4 K for CP, GM, and PS with a lattice spacing $a_0 \in \{0.2, 0.25, 0.5, 1\}$ nm for CP and $a_0 \in \{0.25, 0.5, 1\}$ nm for GM and PS. For CP and PS, our results are in full agreement with the data reported in the literature [58] and shown in Fig. 1(a).

The CGLT is a mean-field approach that ignores thermal fluctuations. Here it is based on nearest neighbor interactions. This differs from the GCMC approach that accounts for thermal fluctuations leading to a lower T_{cc} by $\approx$10 K. This is what we observe for CP compared to those in the literature based on GCMC and CGLT. However, the confinement imposed by GM seems insignificant and independent of

the degree of spatial disorder since $T_{cc} \lessapprox T_c^{3D}$. Let us explore this contrast further.

The PSD in each considered PS has a peak that corresponds to the monodisperse particle radii with no variations around this peak. For the porous solids reported in the literature such as Vycor, the PSD can be captured by a Gaussian fit with a well-pronounced peak representing the mean and a small variance around it [59]. However, the PSD for GM exhibits a wide range and is not well represented by the first moment of the distributions (see Supplemental Material [32]). To further characterize these distributions, we consider the proportion $N_s^f(r)$ of interface solid sites in a spherical domain of radius r, assuming that each site affects the evolution of a given interface fluid site through a connected path in the fluid domain and normalized by the total number of interface solid sites. $N_s^f(r)$ represents the range of fluid-fluid correlations that can develop from the pore surface. Therefore, it contains information regarding correlation length for the adsorbed fluid or surface-surface correlation length. The distributions of $N_s^f(r = 20\ \text{nm})$ as shown in Fig. 1(b),(c) for structure C highlight the difference in confinement experienced by a fluid site in a granular material as opposed to a porous solid. For PS, each distribution is a Gaussian with a sharp peak at the mean and a small variance around it. For GM, the distributions are no longer Gaussian but distributed widely and multimodally, with the largest peak having a lower probability density than their porous solid counterparts. For PS, these distributions imply that every fluid site at the pore-solid interface has a high probability of interacting with a fixed number of solid sites, while this probability is lower and the number of such interactions more widespread for GM. This notion is also reiterated in the partial radial distribution functions for fluid sites at the pore-solid interface interacting with solid sites, as shown in Fig. 1(d).

Thus, this disparity in adsorbed fluid correlation or surface-surface correlation length emerging from "switching" solid curvature leads to more pronounced confinement effects in PS, as opposed to their GM counterparts for which the surface-surface correlation length approaches the fluid-fluid correlation length in the bulk. Our results seem to depart from the Monte Carlo-based study reported in [60] for disordered granular packings with a similar packing fraction, $f_s = 0.386$, as our study observed a more pronounced shift in critical temperature. This can be attributed to space discretization since, in our study, the size ratio between the solid particle diameter ($2R$) and a fluid molecule (σ) is $\approx 40:1$, while in [60] this ratio is $7.055:1$. Thus, our results suggest that bulk fluid behavior prevails in granular media exhibiting at least $2R/\sigma \gtrapprox 40$.

We now turn our focus to capillary pressure fields inside the pore domain Ω_p, defined as all fluid sites with no solid neighbors. Prior to any analyses, the average pressure of the reservoir is subtracted from the capillary pressure field

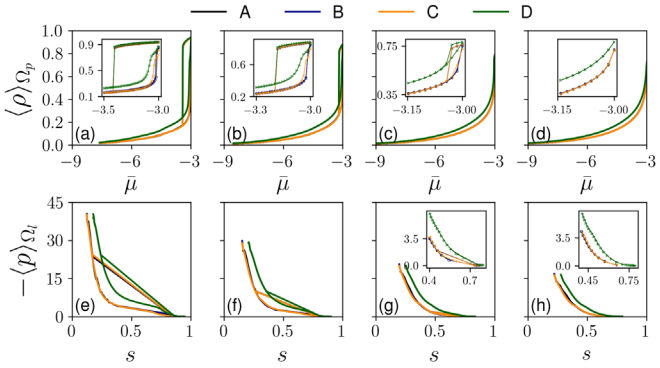

FIG. 2. Isotherms (a)–(d) and capillary pressure curves (e)–(h) for granular packings at $\bar{T} = 1.0$, $\bar{T} = 1.2$, $\bar{T} = 1.4$, and $\bar{T} = 1.5$, respectively.

$p(\vec{x})$. The lattice spacing is chosen based on water-air surface tension $\gamma_{lg} \approx w_{ff}/2a_0 \approx 72$ mN/m at $T = 300$ K and thus $a_0 \sim 0.25$ nm [48], comparable to the size of a water molecule. Having determined T_{cc} associated with these physical parameters and for the granular aggregates considered previously, we simulate capillary condensation and evaporation for $\bar{T} = k_B T/w_{ff} \in \{1.0, 1.2, 1.4, 1.5\}$ with the corresponding adsorption and desorption isotherms, as shown in Fig. 2(a)–(d). The hysteresis loop is present for $\bar{T} \leq 1.4$, but it disappears at $\bar{T} = 1.5$, with its shape becoming less symmetric with increasing temperature, a signature of disordered porous materials. A similar observation regarding the disappearance of the hysteresis loop can be made for CP (see Supplemental Material [32]). Furthermore, there is a jump in mean density at $\bar{T} = 1.4$, while it evolves continuously at $\bar{T} = 1.5$, suggesting a second order phase transition in the latter.

The density fields at a given cross section for various temperatures and for the relative humidity $h = \exp[(\mu - \mu_{\text{sat}}^{3D})/k_B T] = 0.96$ are shown in Fig. 3(a)–(d),

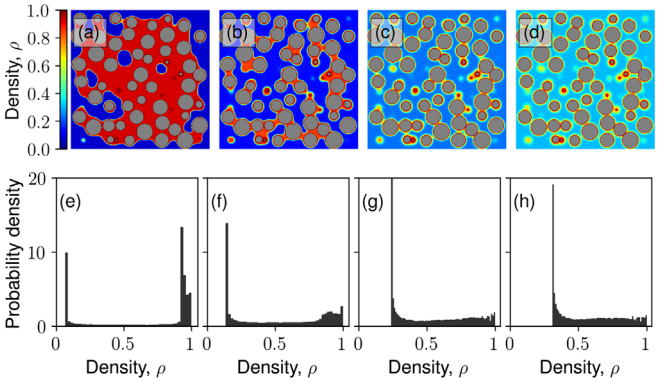

FIG. 3. (a)–(d): spatial distribution of density fields, $\rho(\vec{x})$, for granular packing C and at cross sections corresponding to $z = 44$ nm, $h = 0.96$. (e)–(h): probability density for the density fields (coarse-grained over $L^3 = 1\ \text{nm}^3$) for the same structure at $h = 0.96$ for $\bar{T} = 1.0$, $\bar{T} = 1.2$, $\bar{T} = 1.4$, and $\bar{T} = 1.5$, respectively.

which visualizes the extent of the diffusive interface increasing as $\bar{T} \to \bar{T}_{cc}$. Furthermore, the density distributions at a given h show a bimodal response for $\bar{T} \ll \bar{T}_{cc}$ as expected for a first order phase transition, while its bimodality progressively disappears with increasing $\bar{T}$, i.e., temperature as control parameter, a hallmark of a second order phase transition [see Fig. 3(e)–(h)].

Capillary pressure is a manifestation of phase coexistence. Capillary curves describe the relationship between liquid saturation $s = \langle \rho \rangle_{\Omega_p}$ and capillary pressure $p_c(s) = \langle p \rangle_{\Omega_g} - \langle p \rangle_{\Omega_l}$, where Ω_g and Ω_l denote gas and liquid domains, respectively [61]. Capillary pressure can be estimated from Eq. (2) via the first moment of pressure in the liquid domain, $p_c \approx -\langle p \rangle_{\Omega_l}$, given that $\langle p \rangle_{\Omega_g}$ in the gas domain is relatively negligible. The liquid domain Ω_l is determined via a threshold for local density $\rho(\vec{x}_i)$ with the results for $\rho_{\text{th}} = 0.55$ shown in Fig. 2(e)–(h). The choice of local density threshold does not impact capillary curves significantly (see Supplemental Material [32]). These curves exhibit two distinct regimes: a sharp decrease with s associated with the buildup of adsorbed film on the pore-solid surfaces, followed by a smooth decrease for $\bar{T} \ll \bar{T}_{cc}$. In the vicinity of $\bar{T} \approx \bar{T}_{cc}$, the capillary curves suggest pore filling and emptying at zero capillary pressure with the first regime absent, signaling the termination of phase coexistence [Fig. 2(e)–(h)]. This can also be observed for CP (see Supplemental Material [32]). Furthermore, both the isotherms and capillary curves show no particular dependence on the degree of spatial disorder, although they do display a pronounced dependence on f_s as the behavior pertaining to structure D consistently differs from structures A–C, given that all studied structures, $f_s \in \{0.43, 0.5\}$, can be classified as dilute suspensions. However, the higher order cumulants of the capillary pressure fields are sensitive to spatial disorder (see Supplemental Material [32]).

To further explore the nature of capillary phase transition, we carry out a finite-size scaling (FSS) analysis, and the critical exponents ν and γ governing singularities in correlation length and connected susceptibility are determined for PS and GM. To this end, connected susceptibility $\chi = L^3(\langle \rho^2 \rangle - \langle \rho \rangle^2)$ is computed for volumes of characteristic length L chosen to provide a relatively large number of realizations ($N > 100$) based on the diameter of the particles (pores). For each realization x, $\chi_{\max}(x, L)$ is obtained. From $\chi_{\max}(L) = \langle \chi_{\max}(x, L) \rangle$ and its corresponding chemical potential $\bar{\mu}^*(L) = \langle \bar{\mu}^*(x, L) \rangle$, the critical exponents are estimated and reported in Table I. The quality of the fits are reasonable (see Supplemental Material [32]), but obviously the accuracy increases with a larger number of realizations and a larger set of coarse-graining lengths that span at least a decade. The obtained values of critical exponents lead to a reasonable collapse for the susceptibility curves, with an example shown in Fig. 4.

TABLE I. Critical exponents estimated from FSS.

	A	B	C	D
$(\nu, \gamma)_{\text{GM}}$	(0.68,2.14)	(0.77,2.43)	(0.88,2.89)	(0.81,2.54)
$(\nu, \gamma)_{\text{PS}}$	(0.76,2.21)	(0.82,2.42)	(0.94,2.70)	(0.47,1.39)

With regard to the nature of phase transition near $\bar{T}_{cc}$, our estimations for ν suggest a second order phase transition given its discrepancy with the expected scaling for a first order transition in a mean-field theory, i.e., $\nu \approx 2/d (= 3)$ [45]. This observation combined with the disappearance of the bimodality of the density distribution, at a given h, as temperature increases and the continuous evolution of density near T_{cc} suggest a second order phase transition near T_{cc}. Furthermore, our results for ν and γ are within the range of those reported in the literature for 3D-RFIM for a variety of idealized random fields and consistent with universality of confined colloid-polymer mixture [29,30] with $\nu = 1.1 \pm 0.1$ and $\gamma = 2.02 \pm 0.49$. Additionally, the reported critical exponents, ν and γ, for 3D-RFIM with an underlying Gaussian distribution are $\nu \in [0.96, 1.46]$ and $\gamma \in [1.7, 2.51]$ [62–69], for a double Gaussian distribution $\nu \in [1.33, 2.68]$ and $\gamma \in [1.98, 4.0]$, and for a Poisson distribution $\nu = 1.31 \pm 0.08$ and $\gamma = 1.95 \pm 0.12$ [69]. Given the limited options for coarse-graining lengths and the inherent challenges in extracting critical exponents [30], the agreements between the reported results and those in the literature are very promising. Moreover, we observe that even for the ordered structure A with periodic arrangement of particles (pores), the critical exponents are in agreement with those reported for 3D-RFIM. This is consistent with Brochard and de Gennes's conjecture as the underlying random field is generated by the distribution of a wall separation best captured by the pair distribution functions shown in Fig. 1(d), which highlight the local disorder in fluid-solid interactions. For the isolated spherical voids in the PS, the associated pair distance distribution functions are Gaussians [70], and hence the agreement between the values reported in Table I and those in the literature with underlying Gaussian random fields.

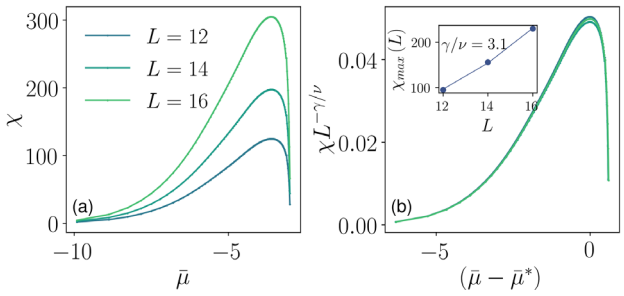

FIG. 4. (a) Susceptibility for structure C and $\bar{T} = 1.5$ for volumes of length $L = 12$ ($N = 217$), $L = 14$ ($N = 126$), and $L = 16$ ($N = 125$). (b) Collapse of the susceptibility curves (inset: a power law fit to estimate γ).

To conclude, we demonstrated that confinement effects are much less pronounced in the studied granular media as opposed to their porous solid counterparts. This was shown to be a consequence of the surface-surface correlation length with a connected path through the fluid domain as captured via the function $N_s^f(r)$ and not necessarily the mean PSD. In granular aggregates, this correlation length approaches that of the bulk fluid, recovering a bulk fluid behavior. At the same time, critical exponents estimated from FSS analysis map GM and PS into the 3D-RFIM as previously hypothesized by Brochard and de Gennes [24,25]. This implies that the universality class can be resolved in the absence of strong confinement, with the underlying effective random field being a consequence of local disorder in fluid-solid interactions captured by their pair distribution function and the associated pair distance distribution function in the pore domain and not necessarily the spatial arrangement of the particles (pores). Furthermore, our results suggest a first order phase transition for $T \ll T_{cc}$ and a second order phase transition for $T \approx T_{cc}$ irrespective of the degree of disorder and the nature of the solid matrix, whether discrete or continuous. This is based on the estimations for critical exponent ν, the evolution of isotherms, the capillary pressure evolution with temperature, and the distribution of density fields. Additionally, from the capillary curves, the termination of phase coexistence occurs at $T \approx T_{cc}$. This implies that T_{cc} represents a true critical temperature that is insensitive to the degree of disorder and the nature of solid matrix.

In the future, the critical behavior of random porous materials should be examined beyond the dilute suspension limit with a stronger degree of heterogeneity, e.g., effective random fields with underlying Lévy stable distributions [71] accounting for chemical disorder and including correlated structures. The scaling properties of the hull of percolation [72–74] can be illuminating in exploring surface-surface correlations in more complex pore domains. Lastly, the role of solid deformability on the nature of liquid-gas phase transition remains to be explored.

The authors would like to thank Professor Mehran Kardar (Department of Physics at MIT) for reviewing the first draft of this paper and providing very insightful suggestions, including carrying out a finite-size scaling analysis. The authors also thank Professor Emanuela Del Gado (Department of Physics at Georgetown University) for reviewing the last draft of this paper before its final version and providing critical feedback incorporated into this final version. S. M. and T. Z. also thank Professor Enrico Masoero (School of Engineering at Newcastle University) for fruitful discussions. T. Z. thanks the Drinkward Fellowship at Caltech's Mechanical and Civil Engineering Department.

*Corresponding author.
monfared@caltech.edu
†tingtaoz@caltech.edu
‡jandrade@caltech.edu
§aikaterini.ioannidou@umontpellier.fr
‖franck.radjai@umontpellier.fr
¶ulm@mit.edu
**Roland.pellenq@cnrs.fr

[1] L. Bocquet, E. Charlaix, S. Ciliberto, and J. Crassous, Moisture-induced ageing in granular media and the kinetics of capillary condensation, Nature (London) **396**, 735 (1998).
[2] M. Scheel, R. Seemann, M. Brinkmann, M. D. Michiel, A. Sheppard, B. Breidenbach, and S. Herminghaus, Morphological clues to wet granular pile stability, Nat. Mater. **7**, 189 (2008).
[3] O. Coussy, *Mechanics and Physics of Porous Solids* (John Wiley & Sons, Ltd, New York, 2010).
[4] M. Ghestem, R. C. Sidle, and A. Stokes, The influence of plant root systems on subsurface flow: Implications for slope stability, BioScience **61**, 869 (2011).
[5] M. Fakih, J.-Y. Delenne, F. Radjai, and T. Fourcaud, Root growth and force chains in a granular soil, Phys. Rev. E **99**, 042903 (2019).
[6] S. Ó. Snæbjörnsdóttir, B. Sigfússon, C. Marieni, D. Goldberg, S. R. Gislason, and E. H. Oelkers, Carbon dioxide storage through mineral carbonation, Nat. Rev. Earth Environ. **1**, 90 (2020).
[7] M. E. Davis, Ordered porous materials for emerging applications, Nature (London) **417**, 813 (2002).
[8] A. U. Czaja, N. Trukhan, and U. Müller, Industrial applications of metal–organic frameworks, Chem. Soc. Rev. **38**, 1284 (2009).
[9] P. Barthelemy, M. Ghulinyan, Z. Gaburro, C. Toninelli, L. Pavesi, and D. S. Wiersma, Optical switching by capillary condensation, Nat. Photonics **1**, 172 (2007).
[10] P. G. de Gennes, Partial filling of a fractal structure by a wetting fluid, in *Physics of Disordered Materials* (Springer US, New York, 1985), pp. 227–241.
[11] M. Thommes and G. H. Findenegg, Pore condensation and critical-point shift of a fluid in controlled-pore glass, Langmuir **10**, 4270 (1994).
[12] L. D. Gelb, K. E. Gubbins, R. Radhakrishnan, and M. Sliwinska-Bartkowiak, Phase separation in confined systems, Rep. Prog. Phys. **62**, 1573 (1999).
[13] R. J.-M. Pellenq and P. E. Levitz, Capillary condensation in a disordered mesoporous medium: A grand canonical Monte Carlo study, Mol. Phys. **100**, 2059 (2002).
[14] J. Puibasset and R. J.-M. Pellenq, Grand canonical Monte Carlo simulation study of water structure on hydrophilic mesoporous and plane silica substrates, J. Chem. Phys. **119**, 9226 (2003).
[15] B. Coasne, F. D. Renzo, A. Galarneau, and R. J. M. Pellenq, Adsorption of simple fluid on silica surface and nanopore: Effect of surface chemistry and pore shape, Langmuir **24**, 7285 (2008).
[16] E. Barsotti, S. P. Tan, M. Piri, and J.-H. Chen, Phenomenological study of confined criticality: Insights from the capillary condensation of propane, n-butane, and n-pentane in nanopores, Langmuir **34**, 4473 (2018).

[17] M. Láska, A. O. Parry, and A. Malijevský, Three-Phase Fluid Coexistence in Heterogenous Slits, Phys. Rev. Lett. **124**, 115701 (2020).

[18] R. Evans, Fluids adsorbed in narrow pores: Phase equilibria and structure, J. Phys. Condens. Matter **2**, 8989 (1990).

[19] K. Binder and D. P. Landau, Capillary condensation in the lattice gas model: A Monte Carlo study, J. Chem. Phys. **96**, 1444 (1992).

[20] R. Valiullin, S. Naumov, P. Galvosas, J. Karger, H. Woo, F. Porcheron, and P. Monson, Exploration of molecular dynamics during transient sorption of fluids in mesoporous materials, Nature (London) **443**, 965 (2006).

[21] A. O. Parry, C. Rascón, N. B. Wilding, and R. Evans, Condensation in a Capped Capillary is a Continuous Critical Phenomenon, Phys. Rev. Lett. **98**, 226101 (2007).

[22] T. D. Lee and C. N. Yang, Statistical theory of equations of state and phase transitions. II. Lattice gas and Ising model, Phys. Rev. **87**, 410 (1952).

[23] H. Stanley, *Introduction to Phase Transitions and Critical Phenomena* (Clarendon Press, Oxford, 1971).

[24] F. Brochard and P. de Gennes, Phase transitions of binary mixtures in random media, J. Phys. Lett. **44**, 785 (1983).

[25] P. G. D. Gennes, Liquid-liquid demixing inside a rigid network. Qualitative features, J. Phys. Chem. **88**, 6469 (1984).

[26] D. Bi, J. Zhang, B. Chakraborty, and R. P. Behringer, Jamming by shear, Nature (London) **480**, 355 (2011).

[27] H. Laubie, F. Radjai, R. Pellenq, and F.-J. Ulm, Stress Transmission and Failure in Disordered Porous Media, Phys. Rev. Lett. **119**, 075501 (2017).

[28] Y. Imry and S. keng Ma, Random-Field Instability of the Ordered State of Continuous Symmetry, Phys. Rev. Lett. **35**, 1399 (1975).

[29] R. L. C. Vink, K. Binder, and H. Löwen, Critical Behavior of Colloid-Polymer Mixtures in Random Porous Media, Phys. Rev. Lett. **97**, 230603 (2006).

[30] R. L. C. Vink, K. Binder, and H. Löwen, Colloid–polymer mixtures in random porous media: Finite size scaling and connected versus disconnected susceptibilities, J. Phys. Condens. Matter **20**, 404222 (2008).

[31] R. L. C. Vink, Critical behavior of soft matter fluids in bulk and in random porous media: From Ising to random-field Ising universality, Soft Matter **5**, 4388 (2009).

[32] See Supplemental Material, which includes Refs. [33–43], at http://link.aps.org/supplemental/10.1103/PhysRevLett.125.255501 for the generation of the disordered structures, derivation of capillary stress tensor, isotherms and capillary curves for cylindrical pores, critical exponents fits and their qualities, sensitivity of capillary curves to local density threshold, and higher order cumulants of the density and pressure fields in the pore domain for the disordered structures.

[33] S. Torquato, *Random Heterogeneous Materials* (Springer, New York, 2002).

[34] H. Laubie, S. Monfared, F. Radjai, R.-M. Pellenq, and F.-J. Ulm, Disorder-induced stiffness degradation of highly disordered porous materials, J. Mech. Phys. Solids **106**, 207 (2017).

[35] S. Plimpton, Fast parallel algorithms for short-range molecular dynamics, J. Comput. Phys. **117**, 1 (1995).

[36] E. Masoero, E. Del Gado, R.-M. Pellenq, F.-J. Ulm, and S. Yip, Nanostructure and Nanomechanics of Cement: Polydisperse Colloidal Packing, Phys. Rev. Lett. **109**, 155503 (2012).

[37] E. Masoero, E. Del Gado, R.-M. Pellenq, F.-J. Ulm, and S. Yip, Nano-scale mechanics of colloidal c-s-h gels, Soft Matter **10**, 491 (2014).

[38] K. Ioannidou, K. Krakowiak, M. Bauchy, C. Hoover, E. Masoero, S. Yip, F.-J. Ulm, P. Levitz, R. Pellenq, and E. Del Gado, Mesoscale texture of cement hydrates, Proc. Natl. Acad. Sci. U.S.A. **113**, 2029 (2016).

[39] C. Rycroft, voro++: A three-dimensional voronoi cell library in c++, Chaos **19**, 041111 (2009).

[40] L. D. Gelb and K. Gubbins, Pore size distributions in porous glasses: A computer simulation study, Langmuir **15**, 305 (1999).

[41] S. Bhattacharya and K. Gubbins, Fast method for computing pore size distributions of model materials, Langmuir **22**, 7726 (2006).

[42] M. Fisher, The renormalization group in the theory of critical behavior, Rev. Mod. Phys. **46**, 597 (1974).

[43] J.-Y. Delenne, V. Richefeu, and F. Radjai, Liquid clustering and capillary pressure in granular media, J. Fluid Mech. **762**, R5 (2015).

[44] E. Kierlik, P. A. Monson, M. L. Rosinberg, L. Sarkisov, and G. Tarjus, Capillary Condensation in Disordered Porous Materials: Hysteresis Versus Equilibrium Behavior, Phys. Rev. Lett. **87**, 055701 (2001).

[45] E. Kierlik, P. A. Monson, M. L. Rosinberg, and G. Tarjus, Adsorption hysteresis and capillary condensation in disordered porous solids: A density functional study, J. Phys. Condens. Matter **14**, 9295 (2002).

[46] P. A. Bonnaud, Q. Ji, B. Coasne, R. J.-M. Pellenq, and K. J. V. Vliet, Thermodynamics of water confined in porous calcium-silicate-hydrates, Langmuir **28**, 11422 (2012).

[47] J. W. Cahn and J. E. Hilliard, Free energy of a nonuniform system. I. Interfacial free energy, J. Chem. Phys. **28**, 258 (1958).

[48] T. Zhou, K. Ioannidou, E. Masoero, M. Mirzadeh, R. J.-M. Pellenq, and M. Z. Bazant, Capillary stress and structural relaxation in moist granular materials, Langmuir **35**, 4397 (2019).

[49] J. W. Gibbs and J. Tyndall, *On the Equilibrium of Heterogeneous Substances: First [-Second] Part* (Connecticut Academy of Arts and Sciences, Connecticut, 1874).

[50] L. Rayleigh, XX. on the theory of surface forces.—II. Compressible fluids, London, Edinburgh, and Dublin, Philos. Mag. J. Sci. **33**, 209 (1892).

[51] D. J. Korteweg, Sur la forme que prennent les équations du mouvements des fluides si l on tient compte des forces capillaires causés par des variations de densité con-sidérables mais connues et sur la théorie de la capillarité dans l hypothése d une variation continue de la densité, Archives Néerlandaises des Sciences exactes et naturelles **6**, 1 (1901), https://ci.nii.ac.jp/naid/10016444962/.

[52] D. Anderson and G. McFadden, Diffuse-interface methods in fluid mechanics, U.S. Department of Commerce, Gathersburg, MD, Technical Report No., NISTIR 6018, 1997.

[53] M. Kruk, M. Jaroniec, J. M. Kim, and R. Ryoo, Characterization of highly ordered MCM-41 silicas using x-ray

diffraction and nitrogen adsorption, Langmuir **15**, 5279 (1999).
[54] C. G. V. Burgess, D. H. Everett, and S. Nuttall, Adsorption of carbon dioxide and xenon by porous glass over a wide range of temperature and pressure-applicability of the langmuir case VI equation, Langmuir **6**, 1734 (1990).
[55] R. Salazar and L. D. Gelb, Application of the Bethe-Peierls approximation to a lattice-gas model of adsorption on mesoporous materials, Phys. Rev. E **71**, 041502 (2005).
[56] I. Brovchenko, A. Geiger, and A. Oleinikova, Water in nanopores. I. Coexistence curves from Gibbs ensemble Monte Carlo simulations, J. Chem. Phys. **120**, 1958 (2004).
[57] J. Puibasset and R.-M. Pellenq, Water confined in mesoporous silica glasses: Influence of temperature on adsorption/desorption hysteresis loop and fluid structure, Eur. Phys. J. Spec. Top. **141**, 41 (2007).
[58] B. Coasne, A. Galarneau, R. J. M. Pellenq, and F. D. Renzo, Adsorption, intrusion and freezing in porous silica: The view from the nanoscale, Chem. Soc. Rev. **42**, 4141 (2013).
[59] P. Levitz, G. Ehret, S. K. Sinha, and J. M. Drake, Porous vycor glass: The microstructure as probed by electron microscopy, direct energy transfer, small-angle scattering, and molecular adsorption, J. Chem. Phys. **95**, 6151 (1991).
[60] K. S. Page and P. A. Monson, Monte Carlo calculations of phase diagrams for a fluid confined in a disordered porous material, Phys. Rev. E **54**, 6557 (1996).
[61] E. Charlaix and M. Ciccotti, Capillary condensation in confined media, *Handbook of Nanophysics* (CRC Press,, Boca Raton, 2009).
[62] B. Ahrens, J. Xiao, A. K. Hartmann, and H. G. Katzgraber, Diluted antiferromagnets in a field seem to be in a different universality class than the random-field Ising model, Phys. Rev. B **88**, 174408 (2013).
[63] M. Picco and N. Sourlas, On the phase transition of the 3D random field Ising model, J. Stat. Mech. 03 (2014) P03019.
[64] Y. Wu and J. Machta, Numerical study of the three-dimensional random-field Ising model at zero and positive temperature, Phys. Rev. B **74**, 064418 (2006).
[65] M. Picco and N. Sourlas, Diluted antiferromagnetic 3D Ising model in a field, Europhys. Lett. **109**, 37001 (2015).
[66] H. Rieger, Critical behavior of the three-dimensional random-field Ising model: Two-exponent scaling and discontinuous transition, Phys. Rev. B **52**, 6659 (1995).
[67] J.-C. A. d'Auriac and N. Sourlas, The 3D random field Ising model at zero temperature, Europhys. Lett. **39**, 473 (1997).
[68] M. E. J. Newman and G. T. Barkema, Monte Carlo study of the random-field Ising model, Phys. Rev. E **53**, 393 (1996).
[69] N. G. Fytas and V. Martín-Mayor, Efficient numerical methods for the random-field Ising model: Finite-size scaling, reweighting extrapolation, and computation of response functions, Phys. Rev. E **93**, 063308 (2016).
[70] D. I. Svergun and M. H. J. Koch, Small-angle scattering studies of biological macromolecules in solution, Rep. Prog. Phys. **66**, 1735 (2003).
[71] *Lévy Flights and Related Topics in Physics*, edited by M. F. Shlesinger, G. M. Zaslavsky, and U. Frisch (Springer Berlin Heidelberg, Berlin, Heidelberg, 1995).
[72] B. Sapoval, M. Rosso, and J. Gouyet, The fractal nature of a diffusion front and the relation to percolation, J. Phys. Lett. **46**, 149 (1985).
[73] M. Rosso, J. F. Gouyet, and B. Sapoval, Gradient Percolation in Three Dimensions and Relation to Diffusion Fronts, Phys. Rev. Lett. **57**, 3195 (1986).
[74] J.-M. Debierre, Hull of Percolation Clusters in Three Dimensions, in *Soft Order in Physical Systems* (Springer US, New York, 1994), pp. 159–162.